

Rotational Characterization of Hayabusa II

Target Asteroid (162173) 1999 JU3

Nicholas A. Moskovitz ^{a,b,1} Shinsuke Abe ^c Kang-Shian Pan ^c

David J. Osip ^d Dimitra Pefkou ^a Mario D. Melita ^e

Mauro Elias ^e Kohei Kitazato ^f Schelte J. Bus ^g

Francesca E. DeMeo ^a Richard P. Binzel ^a Paul A. Abell ^h

^a*Massachusetts Institute of Technology, Department of Earth, Atmospheric and Planetary Sciences, 77 Massachusetts Avenue, Cambridge, MA 02139 (U.S.A.)*

^b*Carnegie Institution of Washington, Department of Terrestrial Magnetism, 5241 Broad Branch Road, Washington, DC 20008 (U.S.A.)*

^c*National Central University, Institute of Astronomy, 300 Jhongda Road, Jhongli, Taoyuan 32001 (Taiwan)*

^d*Carnegie Institution of Washington, Las Campanas Observatory, Colina El Pino, Casilla 601 La Serena (Chile)*

^e*Universidad de Buenos Aires, Instituto de Astronomica y Fisica del Espacio, Buenos Aires (Argentina)*

^f*The University of Aizu, Research Center for Advanced Information Science and Technology, Ikki-machi, Aizu-Wakamatsu, Fukushima 965-8580 (Japan)*

^g*University of Hawaii, Institute for Astronomy, 640 N. A'ohoku Place, Hilo, HI 96720 (U.S.A.)*

^h*NASA Johnson Space Center, Astromaterials Research and Exploration Science Directorate, Houston, TX 77058 (U.S.A.)*

Copyright © 2012 Nicholas A. Moskovitz

Number of pages: 24

Number of tables: 3

Number of figures: 6

¹ Observations conducted while at Carnegie DTM, current address is MIT.

Proposed Running Head:

Rotational characterization of 1999 JU3

Please send Editorial Correspondence to:

Nicholas A. Moskovitz

Department of Earth, Atmospheric and Planetary Sciences

Massachusetts Institute of Technology

77 Massachusetts Avenue

Cambridge, MA 02139, USA.

Email: nmosko@mit.edu

Phone: (617) 253-1268

1 ABSTRACT

2 The Japanese Space Agency's Hayabusa II mission is scheduled to rendezvous
3 with and return a sample from the near-Earth asteroid (162173) 1999 JU3.
4 Previous visible-wavelength spectra of this object show significant variability
5 across multiple epochs which could be the result of a compositionally hetero-
6 geneous surface. We present new visible and near-infrared spectra to demon-
7 strate that thermally altered carbonaceous chondrites are plausible compo-
8 sitional analogs, however this is a tentative association due to a lack of any
9 prominent absorption features in our data. We have also conducted a series of
10 high signal-to-noise visible-wavelength observations to investigate the reported
11 surface heterogeneity. Our time series of visible spectra do not show evidence
12 for variability at a precision level of a few percent. This result suggests two
13 most likely possibilities. One, that the surface of 1999 JU3 is homogenous and
14 that unaccounted for systematic effects are causing spectral variation across
15 epochs. Or two, that the surface of 1999 JU3 is regionally heterogenous, in
16 which case existing shape models suggest that any heterogeneity must be lim-
17 ited to terrains smaller than approximately 5% of the total surface area. These
18 new observations represent the last opportunity before both the launch and
19 return of the Hayabusa II spacecraft to perform ground-based characteriza-
20 tion of this asteroid. Ultimately, these predictions for composition and surface
21 properties will be tested upon completion of the mission.

22 *Keywords:* Asteroids; Asteroids, rotation; Asteroids, composition; Photome-
23 try; Spectroscopy

24 1 Introduction

25 In June of 2010 the Japanese Space Agency’s Hayabusa mission successfully
26 completed the first ever sample return from an asteroid (Fujiwara et al., 2006;
27 S. Abe et al., 2006; Nakamura et al., 2011, and references therein). The success
28 of this mission has spawned a successor, Hayabusa II, which is scheduled to
29 rendezvous with and return a sample from the asteroid (162173) 1999 JU3.
30 This object was discovered by the Lincoln Near-Earth Asteroid Research (LIN-
31 EAR) survey on 1999 May 10. It is an Apollo-class near-Earth asteroid with
32 one of the lowest values of Δv for any object with an absolute magnitude
33 less than $H=20$ ², and is thus a highly favorable space mission target. The
34 current Hayabusa II timeline proposes a launch in 2014 or 2015, rendezvous
35 with the asteroid in 2018, and return of a sample to Earth in 2020. Like its
36 predecessor this mission provides the opportunity to directly test the validity
37 of ground-based analytical techniques with pre-encounter predictions for the
38 physical and chemical properties of the asteroid (e.g. Binzel et al., 2001b).

39 Previous observations of 1999 JU3 were conducted following its discovery in
40 1999 and during its favorable apparition in 2007. Ground-based photometry
41 determined a light curve period of about 7.63 hours (Abe et al., 2008; Müller
42 et al., 2011), which has since been confirmed with photometry from the 2012
43 apparition (Kim et al., 2012). A weighted average of space and ground-based
44 observations in the mid-infrared suggest an effective diameter of 870 ± 30
45 meters and an albedo of $6.954 \pm 0.005\%$ (Hasegawa et al., 2008; Campins et
46 al., 2009; Müller et al., 2011). Prior to the present study, visible-wavelength
47 spectra had been obtained in May 1999, July 2007, and September 2007 (Fig-
48 ure 1, Table 1). These data display marked variability in spectral slope and in

² http://echo.jpl.nasa.gov/~lance/delta_v/delta_v.rendezvous.html

the presence of absorption features. The spectrum from 1999 shows UV absorption short-ward of about $0.65\ \mu\text{m}$ and a featureless neutral slope at longer wavelengths (Binzel et al., 2001a). The July 2007 data, which suffer from the lowest signal-to-noise, show an overall red slope with a pronounced absorption feature $\sim 10\%$ deep centered between 0.6 and $0.7\ \mu\text{m}$ (Vilas, 2008). The September 2007 spectrum is a combination of data from two nights (Table 1) and is largely featureless with neutral slope (Vilas, 2008). Though these three spectra are broadly consistent with taxonomic classification in the C-complex, such pronounced variability, in this case at the level of $\sim 10\%$, is highly unusual.

This spectral variability has been attributed to a compositionally heterogeneous surface (Vilas, 2008). The absorption feature between 0.6 and $0.7\ \mu\text{m}$ in the July 2007 spectrum was linked to $\text{Fe}^{2+} \rightarrow \text{Fe}^{3+}$ charge transfer transitions in iron-bearing phyllosilicates. The absence of this feature in the May 1999 and September 2007 spectra suggests a non-uniform distribution of these aqueous alteration byproducts. The possible existence of hydrated minerals on the surface of 1999 JU3 is of considerable interest for the purposes of mission planning and the potential sampling of primitive Solar System material. Such surface heterogeneity could be inherited from the asteroid's parent body or could be exogenous in origin, as is believed to be the case for the "black boulder" seen by Hayabusa I on Itokawa (Fujiwara et al., 2006) and for the dark material imaged by the Dawn spacecraft on 4 Vesta (Reddy et al., 2012a).

We present observations of 1999 JU3 from the 2012 apparition, the last favorable observing window before both the scheduled launch and return of the Hayabusa II spacecraft. Visible and near-infrared spectra were obtained to constrain the composition of the asteroid and to investigate claims of a

75 non-uniform surface. Other investigators obtained visible spectra during the
76 2012 observing window (Sugita et al., 2012; Vilas, 2012; Lazzaro et al., 2013).
77 These other data are not directly addressed here, though we note that none of
78 these works found evidence for a $0.7\ \mu\text{m}$ absorption feature or any repeatable
79 spectral variability through multiple rotation periods. We also present here
80 new visible-wavelength photometry to constrain the rotational phases of the
81 asteroid accessed by the 2012 spectroscopic observations. Our observations
82 and reduction techniques are presented in Section 2. Analysis of these data
83 are presented in Section 3. We summarize and discuss the results in Section
84 4.

85 2 Observations and Data Reduction

86 Data presented here were taken with seven different instruments at six tele-
87 scopic facilities and include visible and near-infrared spectroscopy, and visible-
88 wavelength photometry. With the exception of one near-infrared spectrum
89 from 2007, all data were obtained between October of 2011 and July of 2012.
90 Tables 1 and 2 summarize the observing circumstances.

91 2.1 Visible-Wavelength Spectroscopy: LDSS3

92 New visible wavelength spectra were obtained with LDSS3 at the Magellan
93 Clay 6.5m telescope on the nights of UT 2012 June 1-3, coinciding with the
94 opposition of the asteroid at a phase angle of 0.2° on UT June 1 at 07:30. The
95 instrument was operated with a $1.5''$ -wide and $4'$ -long slit and its VPH-All
96 grism. These settings produced a single-order spectrum with a useful spectral
97 range of $0.44\text{-}0.94\ \mu\text{m}$ at an average resolution of about 430 and a dispersion of

1.89 Å/pixel. Each individual spectrum represents a set of 4 x 180s exposures, split between two different nod positions approximately 20" apart along the slit.

Solar analog stars were observed several times throughout each night for calibration purposes (Table 1). With the exception of HD149182, the calibration stars were selected from a list of well-vetted analogs that were used extensively throughout the SMASS survey (Bus and Binzel, 2002). HD149182 was also included because of its close proximity ($< 10^\circ$) to the asteroid and was selected based on its photometric colors and G2V spectral classification. The high degree of consistency amongst our measured spectra (Section 3.2) confirms that HD149182 is a good solar analog.

Reduction of these spectra employed standard IDL and IRAF routines, including a set of IRAF tools developed specifically for LDSS3. Combined He, Ne and Ar arc lamp spectra were obtained at the beginning and end of each night to provide dispersion solutions. Exposures of a white screen illuminated by a quartz lamp were used for flat field calibration.

The extracted asteroid spectra were divided by each of the solar analogs (typically ~ 10 individual observations of solar analogs throughout the night). The best solar analog for a given asteroid spectrum was chosen based on minimization of residual telluric features long-wards of $\sim 0.7 \mu\text{m}$. After division by an analog, individual points in the spectra were then rejected based on a $0.25 \mu\text{m}$ boxcar sigma-clipping routine with a prescribed cutoff of 3 sigma. In all cases less than 10% of the data points were rejected and those that were removed were predominantly distributed at the extremes of the spectra outside the useful spectral range of 0.44-0.94 μm . Generally, less than 10 pixels were removed from within this final trimmed spectral range. After cleaning,

the asteroid spectra were then re-binned by a factor of 13 pixels to produce a dispersion interval very close to $0.0025 \mu\text{m}$ per channel, similar to that of the 1999 spectrum (Binzel et al., 2001a) and a factor approximately 3 times than that of the 2007 data (Vilas, 2008). The error bar on each binned dispersion element was set to the standard deviation of the original 13 pixels. The data were finally normalized at $0.55 \mu\text{m}$ to produce relative reflectance spectra (Figure 1).

The wavelength-averaged signal-to-noise ratio (S/N) of these spectra vary from ~ 60 on the first night (A, B in Figure 1), to ~ 30 on the second night (C), to ~ 20 on the third night (D, E, F). Since exposure times were held constant, this drop in S/N is likely caused by several effects. First, spectra A and B were taken at solar phase angles less than 1° (Table 1) and thus may have captured an opposition surge in brightness. Second, the moon was both waxing and increasingly close to the target throughout the run (Table 1), thus causing a progressive increase in background flux. Third, the target's geocentric and heliocentric distances were both increasing, causing a drop in brightness across the three nights.

2.2 Near-Infrared Spectroscopy: FIRE and SpeX

Near-infrared spectra were obtained in June and July of 2012 with FIRE at the Magellan Baade 6.5m telescope and in September 2007 with SpeX (Rayner et al., 2003) at NASA's Infrared Telescope Facility (IRTF; Table 1). FIRE was operated in its high-throughput prism mode with a $0.8 \times 50''$ slit. These settings produced single-order spectra at a resolution of approximately 400 from 0.8 to $2.45 \mu\text{m}$. Individual exposures were limited to 180s to avoid saturation of telluric emission features and of thermal emission from the instrument and

149 telescope at wavelengths longer than about $2.2\ \mu\text{m}$. Exposures were obtained
150 in ABBA sequences with the object offset along the slit by $9''$ for each nod
151 position. On UT 2012 June 5 a total of $4 \times 180\text{s}$ exposures were obtained. On
152 UT 2012 July 10, when the asteroid was nearly 2 magnitudes fainter, a total
153 of $18 \times 180\text{s}$ exposures were obtained.

154 At the IRTF, SpeX was configured in its low resolution ($R = 250$) prism mode
155 with a $0.8''$ slit for wavelength coverage from 0.8 to $2.5\ \mu\text{m}$. All observations
156 were made with the telescope operating in a standard ABBA nod pattern
157 with individual exposures of 120s . On UT 2007 September 18 a total of 40
158 individual exposures were obtained, on UT 2007 September 20 a total of 50
159 individual exposures were obtained.

160 For both near-infrared spectrographs the slit mask was oriented along the par-
161 allactic angle at the start of each observation to minimize the effects of atmo-
162 spheric dispersion. As with the visible-wavelength spectra, solar analogs were
163 observed to correct for telluric absorption and to remove the solar spectrum
164 from the measured reflectance (Table 1). Reduction of the SpeX data followed
165 Sunshine et al. (2004), reduction of the FIRE data employed an IDL package
166 designed for the instrument and based on the Spextool pipeline (Cushing et
167 al., 2004).

168 A composite visible/near-infrared spectrum of 1999 JU3 is shown in Figure
169 2. The asteroid is a C-type in the DeMeo et al. (2009) taxonomic system.
170 The visible portion is a weighted average of the six LDSS3 spectra in Figure
171 1. The near-infrared portion is a weighted average of the SpeX and FIRE
172 data, and thus represents a combination of data across multiple epochs. Other
173 than some variability in slope, no significant differences were seen amongst
174 the near-infrared spectra within the S/N of the data.

175 2.3 *Visible-Wavelength Photometry: IMACS, Lulin, Tenagra II, and Bosque*
176 *Alegre*

177 Photometric observations (Table 2) were conducted with IMACS at the Mag-
178 ellan Baade 6.5m telescope at Las Campanas Observatory in Chile, with a
179 Princeton Instruments EEV 1k CCD at the Lulin 1m telescope in Taiwan,
180 with a SITe 1k CCD at the Tenagra II 0.81m telescope in Arizona, and with a
181 Tektronics 1k CCD at the Bosque Alegre 1.5m telescope in Argentina. These
182 data were taken on ten separate nights between October 2011 and June 2012.

183 IMACS was operated using the $f/2$ camera, which has a 27.5' field-of-view
184 covered by a mosaic of eight 2k x 4k CCDs with plate scales of 0.2 "/pixel.
185 We employed only one of the eight chips with a subraster about 400x400" in
186 size. We used a Bessell R-band filter with exposure times of 60 seconds. These
187 observations spanned approximately 3 hours per night over three consecutive
188 nights. The Princeton Instruments CCD at Lulin Observatory has a roughly
189 11' field of view with a plate scale of 0.516 "/pixel. These observations were
190 conducted with a Johnson-Cousins R-band filter over the course of approxi-
191 mately 2 hours on a single night. Exposure times were set to 300 seconds. The
192 SITe 1k CDD at the Tenagra II telescope has a 14.8' field-of-view with a plate
193 scale of 0.87 "/pixel. A Johnson-Cousins R-band filter was used. These ob-
194 servations spanned approximately 4.5 hours per night over 4 non-consecutive
195 nights with individual exposure times set to 360 seconds. The Tektronics 1k
196 at the Bosque Alegre 1.5m has a plate scale of 0.33 "/pixel and a field-of-view
197 of 5.7'. Observations were conducted with a Johnson R-band filter, spanning
198 approximately 3.5 hours on two consecutive nights. Exposure times were 240
199 seconds the first night and 200 seconds the second.

200 Reduction of these data employed standard IRAF procedures. Aperture pho-
201 tometry was performed with aperture radii roughly 4 times the measured
202 seeing and a background annulus equal to twice that separation. Some indi-
203 vidual exposures were rejected based on contamination from nearby field stars.
204 Photometric calibration was achieved for the IMACS data with observations
205 of the RU 149 Landolt standard field (Landolt, 1992). All other photometry
206 was performed differentially relative to at least one half dozen on-chip field
207 stars and then scaled to match the calibrated IMACS data. A full table of the
208 collected photometry is included in the online Supplementary Data.

209 **3 Rotational and Compositional Analyses**

210 Our visible-wavelength photometry is used to construct a phase-folded rota-
211 tional light curve of 1999 JU3. This provides the means to constrain the specific
212 rotational phases accessed by the spectroscopic observations and to quantita-
213 tively address the previously reported surface heterogeneity. The combined
214 visible/near-IR spectrum is used to place preliminary constraints on compo-
215 sition.

216 *3.1 Rotational Light Curve*

217 Müller et al. (2011) find a rotation period for 1999 JU3 of 7.63 ± 0.01 hours
218 and Kim et al. (2012) find a period of 7.625 ± 0.003 hours. We use these
219 periods as a guide to phase-fold our broadband photometry (Figure 3). The
220 highest S/N data came from the three nights of observations at Magellan
221 (Table 2). The magnitudes of all other observations are scaled to the mean
222 value of the photometrically calibrated Magellan data. As with previous light

curve measurements (Müller et al., 2011; Kim et al., 2012), our data suggest a small peak-to-peak amplitude of about 0.2 magnitudes. Attempts have been made to exclude data points contaminated by background field stars, however the low galactic latitude of the asteroid ($< 20^\circ$ for all observations) certainly adds to the scatter in the measured photometry.

The light curve in Figure 3 has been phase folded with a synodic period of 7.631 hours relative to the first IMACS observation on UT 2012-04-05 at 06:40 (JD 2456022.778). Light time corrections have been applied relative to this first IMACS observation. This light curve is wrapped such that the first and last few points are repeated at phases < 0 and > 1 . Robustly fitting a light curve period is difficult because the photometric errors are comparable to the amplitude of the light curve and our best quality photometry from IMACS does not span a full rotation period. A unique period is not found when employing the Fourier analysis of Polishook et al. (2012). Thus we attempt to manually constrain the period based on three features in the IMACS data: a subtle peak at phase $= 0.2$, a minimum at phase $= 0.4$ and another peak around phase $= 0.6$. The period is adjusted in increments of 0.001 hours until these three features are roughly aligned for all data. We find that these features are not aligned for periods within ± 0.005 hours of 7.631 hours. This result is consistent with the range of periods suggested by Müller et al. (2011) and Kim et al. (2012), but is not meant to be a more accurate determination.

3.2 *Non-detection of Spectroscopic Variability*

The phase folded light curve is used to provide rotational context for each of the new spectroscopic observations (Figure 3). This phase folding demonstrates that rotational coverage was obtained over approximately 60% of the

asteroid’s surface at a longitudinal sampling of $\sim 45^\circ$. The spectroscopic observations from previous epochs (Binzel et al., 2001a; Vilas, 2008) are not included in Figure 3 because current best estimates for the rotation period (e.g. Kim et al., 2012) still have an associated error that is large enough to preclude linking observations separated by several years.

We compute reflectance ratios to investigate the possibility of a heterogenous surface (Figure 4). These ratios are computed by median combining spectra A through F and then dividing that median into each of the individual spectra. Any deviations from a flat line would indicate the presence of a heterogenous surface. Typical deviations are around 1%, with the largest (just under 4%) seen at the bluest wavelengths in spectrum C. However, all deviations fall within the S/N of the data and thus suggest that the regions on the surface accessed by our observations are homogenous to within a few percent.

Previously reported spectroscopic variability around $0.8\ \mu\text{m}$ (Lazzaro et al., 2013) is not seen in our data set. This non-detection suggests the possibility raised by these authors, that it may be attributed to either instrumental optical fringing or residual effects from the telluric water absorption band centered near $0.8\ \mu\text{m}$.

The rotational context for these spectroscopic data provides a test of our observation and reduction techniques. Figure 3 shows that spectra A and F were obtained at nearly identical rotation phases. The fact that these spectra are indistinguishable (Figure 4), but taken on different nights and calibrated with different solar analogs (Table 1), is a nice validation of the consistency of our methodology.

273 Shape models of 1999 JU3 based on photometry from 2007 have been inde-
 274 pendently developed by Kawakami et al. (2010) and Müller et al. (2011). In
 275 both cases, the small amplitude of the light curve produces nearly spherical
 276 shapes. These models are based upon different data sets, but because of is-
 277 sues of low S/N, do not offer a single unique solution. Unsurprisingly then,
 278 neither shape model produces light curves that match our data well (Figure
 279 3). Clearly the development of a new shape model that fits photometry from
 280 2007 and 2012 is an important task for future work. Due to this ambiguity it
 281 is difficult to absolutely state the surface latitudes and longitudes accessed by
 282 the full ensemble of spectroscopic observations dating back to 1999. However
 283 we can compare model predictions for the spectroscopically accessed surface
 284 regions to illustrate the plausible spatial extent of any non-uniform surface
 285 features.

286 The spectra of 1999 JU3 from September 2007 are fully consistent with the
 287 new data presented here (Figure 1). Any surface heterogeneity must then
 288 be restricted to regions accessed by the observations in May 1999, when the
 289 asteroid displayed UV absorption short-ward of about $0.65\ \mu\text{m}$ (Binzel et al.,
 290 2001a) and in July 2007 when the asteroid showed a prominent absorption
 291 feature between 0.6 and $0.7\ \mu\text{m}$ (Vilas, 2008). These regions would have to
 292 be limited in extent to avoid violating the lack of absorption features in the
 293 other spectra.

294 Table 3 presents the two sets of predicted sub-observer latitudes and longitudes
 295 for all visible-wavelength spectroscopic observations. Figure 5 illustrates the
 296 sub-observer points predicted by the two shape models. Though these sub-

297 observer points are not meant to be absolute and may change with future
 298 improvements to the shape model, their relative separations are informative.
 299 In particular, we are most interested in the distance that separates the sub-
 300 observer points for featureless spectra (September 2007, June 2012) from the
 301 sub-observer points for spectra that display absorption bands (May 1999, July
 302 2007; B and V in Figure 5). We can roughly calculate the physical distance
 303 between sub-observer points by assuming a spherical body with a diameter of
 304 870m, a reasonable approximation for this asteroid (Kawakami et al., 2010;
 305 Müller et al., 2011). The physical distance between sub-observer points is then
 306 just the distance along the great circle that connects these points.

307 According to the Kawakami et al. (2010) model, the observations from May
 308 1999 were taken at a sub-observer point about 180m away from the next closest
 309 point which corresponds to spectrum F (June 2012). And the observations
 310 from July 2007 correspond to a sub-observer point about 160m away from
 311 the September 2007 spectra. According to the Müller et al. (2011) model,
 312 the observations from May 1999 were taken about 140m from the September
 313 2007 points, and the observations from July 2007 correspond to a sub-observer
 314 point about 200m away from spectrum D (June 2012). Taken as a whole, and
 315 independent of which shape model is employed, these calculations suggest
 316 that the reported spectroscopic variability would be a consequence of regional
 317 surface heterogeneity on spatial scales smaller than about 400m in extent
 318 (200m in radius). Regions of this size would occupy about 5% of the asteroid's
 319 total surface area.

320 The ambiguity in shape models emphasizes that rotational information is not
 321 correlated over multiple years. This is indicated by the horizontal bands in Fig-
 322 ure 5. The sub-observer points for those spectra with absorption features could

lie anywhere along these bands. This provides some freedom for the spectrally anomalous regions to “hide” in the gaps between those sub-observer points corresponding to featureless spectra. However, the sub-observer points for both the Binzel et al. (2001a) and Vilas (2008) spectra would have to be shifted by very specific amounts to reconcile the full suite of visible spectra. This issue is further complicated upon consideration of the sub-observer hemispherical footprints of our spectroscopic observations (see online Supplementary Figure A). These footprints indicate that we accessed a significant majority of the surface, leaving very little surface area in which spectroscopically anomalous regions could exist.

3.4 *Compositional Analogs*

With the full visible/near-infrared spectrum (Figure 2) we can make preliminary statements about the composition of 1999 JU3. However, these statements must be interpreted with some skepticism due to the lack of prominent absorption features and issues of degenerate compositional interpretations when dealing with such featureless spectra (e.g. Vernazza et al., 2009; Reddy et al., 2012b,c). A preliminary attempt at compositional analysis is justified by the potential for predictions to be directly tested with a returned sample. We base this analysis solely on our new observations; see Vilas (2008) for an interpretation of previous visible-wavelength spectra.

Our visible and near-infrared spectra confirm a C-type taxonomic classification, but show no evidence for the previously detected 0.7 micron phyllosilicate band (Vilas, 2008) or a prominent UV drop-off short-wards of about 0.65 μm (Binzel et al., 2001a). The data may indicate weak bands around 0.9 μm and short-ward of 0.7 μm , but these features are near the limit of the S/N and

are not robust detections. Without any strong features to directly analyze we employ spectral matching techniques to constrain plausible compositional analogs. Comparison spectra were obtained from a July 2012 release of Brown University’s RELAB database (Pieters, 1983) containing reflectance spectra for just over 17,000 samples. Our search began by selecting only those samples with a spectral range overlapping that of the asteroid and only those samples with an albedo within 5% of that measured for 1999 JU3. This narrowed the list of comparison spectra to 8024 samples. For each of these, either the asteroid or the meteorite data were interpolated to match the wavelengths of the spectrum with the smallest dispersion interval. Both spectra were then normalized at the minimum asteroid wavelength ($0.44\ \mu\text{m}$) before a reduced χ^2 difference was calculated.

The two meteorite spectra with the lowest χ^2 values are shown in Figure 2. These meteorites are a thermally altered sample of the CM carbonaceous chondrite Murchison and the unusual CI chondrite Yamato 86029. The reduced χ^2 values for these meteorites were 2.89 and 3.25 respectively. These were clearly the best fits as the next lowest χ^2 was 6.75 for a sample of a mid-ocean ridge basalt (RELAB ID RB-CMP-023) that was ground to particle sizes 125-250 μm . This spectrum of oceanic basalt matched the general slope of 1999 JU3 but showed a subtle 1 μm absorption band and thus is unlikely to be a good analog.

The mean albedos of the two best-fit samples (6% for Murchison, 3% for Yamato) are by design of the search algorithm close to the $\sim 7\%$ measured for 1999 JU3 (Hasegawa et al., 2008; Campins et al., 2009; Müller et al., 2011). The two best-fit spectra both correspond to the smallest available particle size sorting, $< 63\ \mu\text{m}$ for Murchison and $< 125\ \mu\text{m}$ for Yamato. The Murchison spectrum

374 represents one in series of heating experiments where the temperature of the
 375 sample was raised in increments of 100°C from 300-1000°C (Hiroi et al., 1996).
 376 At each temperature increment a reflectance spectrum was measured. Heat-
 377 ing was shown to reduce spectral slope and decrease the depth of absorption
 378 bands. The Murchison spectrum corresponding to a temperature of 900°C was
 379 the closest match to 1999 JU3. Yamato 86029 has unusual textural properties
 380 and a chemical composition indicative of a rare class of CI chondrites that ex-
 381 perience moderate thermal alteration at temperatures of 500-600°C (Tonui
 382 et al., 2003). 1999 JU3 has been previously linked to carbonaceous chondrites
 383 (Vilas, 2008; Lazzaro et al., 2013), the analysis here expands upon these re-
 384 sults by specifically identifying thermally altered samples as the best available
 385 spectral analogs.

386 4 Discussion

387 We have presented new observations of the Hayabusa II target asteroid 1999
 388 JU3 taken during the favorable 2012 apparition, the last opportunity before
 389 both the launch and return of the spacecraft to perform ground-based char-
 390 acterization. Visible wavelength photometry was used to produce a rotational
 391 light curve. A period of 7.631 ± 0.005 hours and a small amplitude of a few
 392 tenths of a magnitude are consistent with independent light curve measure-
 393 ments (Müller et al., 2011; Kim et al., 2012). Visible and near-infrared spectra
 394 were used to constrain taxonomy and composition. The asteroid is a C-type in
 395 the DeMeo et al. (2009) taxonomic system and the best spectral analogs are
 396 thermally altered carbonaceous chondrites. However, the lack of any promi-
 397 nent absorption features makes this compositional association tentative. High
 398 quality spectra that extend into the near-UV (0.3-0.4 μm) or the 3 μm region

could provide further compositional clues if diagnostic absorption bands are detected (e.g. Hiroi et al., 1993; Rivkin et al., 2002) and may serve as a test of the collisional and thermal evolution of primitive asteroid types (Vilas and Sykes, 1996).

The putative link to carbonaceous chondrites and particularly those that are thermally altered is interesting and merits some preliminary speculation. CM and CI chondrites are primitive meteorites with appreciable quantities of organics and water of hydration (Cloutis et al., 2011a,b). The possible return of such samples would be relevant to issues of astrobiology and to understanding primordial chemistry in the solar nebula (e.g. Morbidelli et al., 2000). The suggested link to heated carbonaceous chondrites could imply that surface temperatures on 1999 JU3 were significantly higher at some point in its past. There is roughly a 50% probability that the chaotic orbital evolution of 1999 JU3 resulted in a perihelion inside of 0.5 AU (its current perihelion distance in 0.96 AU), which translates to surface temperatures of approximately 500 K (Marchi et al., 2009; Michel and Delbó, 2010). This is comparable to the in-situ alteration temperatures experienced by Yamato 86029, but is less than the 900°C experienced by the Murchison sample. Nevertheless, this highlights that thermally altered primitive meteorites could be relevant to understanding the composition of 1999 JU3. Ultimately, the results from Hayabusa II will provide the first-ever direct test of such compositional interpretations from largely featureless asteroid spectra.

We have also presented a time series of visible spectra to address previously reported spectroscopic variability (Vilas, 2008; Lazzaro et al., 2013). Our spectra show no variability at the level of a few percent. There are several possible explanations for this non-detection. First, the asteroid’s surface may be spec-

425 troscopically and compositionally uniform, in which case some unaccounted
 426 for systematic effects would be the cause of spectral variation across epochs.
 427 The hemispherical footprints of our spectral observations cover nearly the en-
 428 tire surface of the asteroid (Supplementary Figure A), thus supporting this
 429 hypothesis. Variations in spectral slope are common with asteroid observa-
 430 tions and can be attributed to observational issues such as weather, phase
 431 angle (Sanchez et al., 2012; Reddy et al., 2012d), or the use of imperfect solar
 432 analogs, but it is unclear how these issues would result in variable absorption
 433 features. Other than a moderately high airmass of ~ 1.9 for the Binzel et
 434 al. (2001a) spectrum, we find no obvious observational reasons why the two
 435 spectra with absorption features should be different.

436 Multi-epoch spectral variability could alternatively be linked to recent alter-
 437 ation events that induced global or near global changes in surface properties.
 438 Planetary encounters (Binzel et al., 2010) or impacts (Richardson et al., 2004)
 439 can alter reflectance properties, however these seem unlikely because two such
 440 events would be required in just 13 years to explain the observed spectroscopic
 441 variability from 1999 to 2007 to 2012.

442 A final explanation is that the surface of 1999 JU3 is in fact heterogenous.
 443 In this case spectral variability could result from the obscuration of surface
 444 regions by local topography as a consequence of changing viewing aspect.
 445 However, the orbital longitudes of both the Earth and the asteroid were very
 446 similar during the May 1999 and June 2012 observations. This would then
 447 require a highly irregular shape (i.e. large topographic relief) to result in sig-
 448 nificant obscuration and spectral variability. A highly irregular shape is in-
 449 consistent with current shape models (Kawakami et al., 2010; Müller et al.,
 450 2011). Therefore, spectral variability caused by a non-uniform surface would

451 have to be attributed to rotational effects. The combination of rotational data
 452 and time resolved spectra provides a means to address this possibility. Exist-
 453 ing shape models (Kawakami et al., 2010; Müller et al., 2011) suggest that
 454 the maximum physical separation of sub-observer points for the full ensemble
 455 of spectroscopic data is about 200 meters (assuming that the asteroid is 870
 456 meters in diameter; Figure 5). Therefore any surface heterogeneity must be
 457 confined to regions no larger than about 400 meters in extent, which corre-
 458 sponds to a size independent surface area fraction of around 5%. However, we
 459 note again that current shape models do not predict light curves consistent
 460 with photometry across multiple epochs. Therefore, the analysis here con-
 461 strains the *plausible* spatial extent of non-uniform surface features, improved
 462 shape models will be required to refine the spectroscopically accessed terrains
 463 indicated in Figure 5.

464 Few asteroids, particularly sub-km objects like 1999 JU3, have been so ex-
 465 tensively observed across multiple epochs. However, non-uniform surfaces are
 466 generally believed to be rare. The long-time exception is asteroid 4 Vesta, one
 467 of very few objects where variability over multiple rotation periods has been
 468 confirmed with remote observations. Vesta displays regional and hemispheri-
 469 cal color heterogeneity, in some cases well in excess of several 10's of percent
 470 (e.g. Bobrovnikoff, 1929; Gaffey, 1997; Reddy et al., 2012a). However, Vesta
 471 is much larger than 1999 JU3, is a different spectral class, and thus may not
 472 be the best object for comparison.

473 There have been reports of rotational spectroscopic heterogeneity amongst
 474 C-class asteroids. For instance, 10 Hygiea, 105 Artemis, 135 Hertha, and 776
 475 Berbericia each show variability at levels less than about 5% in the depths of
 476 their $0.7\ \mu\text{m}$ features (Rivkin et al., 2002; Vilas, 2008). Detecting such subtle

477 variability is intrinsically difficult and as far as we are aware remains to be veri-
478 fied for any asteroid over multiple rotation periods. Asteroid 21 Lutetia, which
479 was visited by the Rosetta spacecraft, shows variability in visible-wavelength
480 spectral slope at the level of a few percent (Barucci et al., 2012). The S/N of
481 our data for 1999 JU3 may be insufficient to detect such muted variability.
482 But again, these examples of spectral variability occur on asteroids that are
483 much larger than 1999 JU3.

484 The former target of the European Space Agency’s Marco Polo mission (175706)
485 1996 FG3 and asteroid 25143 Itokawa, the target of the Hayabusa I mission,
486 are examples of well-studied asteroids in a size regime closer to that of 1999
487 JU3. 1996 FG3 shows prominent (~ 10 ’s of percent) spectral variability in the
488 near-IR (de León et al., 2011). The origin of this variability remains a mystery.
489 Itokawa displays up to 15% color variability on its surface (Saito et al., 2006;
490 M. Abe et al., 2006). This non-uniformity is limited to regions on the order of
491 10’s to 100 meters in extent or at most a few percent of Itokawa’s surface area.
492 This extent is similar to the constraints we have placed on 1999 JU3’s surface,
493 though it remains unclear whether such small regions could significantly in-
494 fluence ground-based observations that only capture hemispherical averages.
495 Ground-based observations of Itokawa prior to arrival of Hayabusa I did not
496 exhibit any variability (Binzel et al., 2001b; Abell et al., 2007).

497 For now, the issue of heterogeneity on the surface of 1999 JU3 remains an
498 open question that may find some resolution from updated shape models. The
499 arrival of the Hayabusa II spacecraft will ultimately determine whether the full
500 ensemble of visible spectra are truly indicative of a non-uniform surface. More
501 generally, the possibility of multiple planetary missions to near-Earth asteroids
502 in the coming decades will provide an opportunity to further investigate the

503 extent of surface heterogeneity on sub-km asteroidal bodies, and thus provide
504 clues about formational and evolutionary processes in the Solar System.

505 **Acknowledgements**

506 We are grateful to Vishnu Reddy and Faith Vilas for their insightful reviews.
507 We thank David Polishook for his helpful input on the lightcurve analysis.
508 This work includes data obtained at the Magellan 6.5m telescopes located at
509 Las Campanas Observatory in Chile and at NASA's IRTF located on Mauna
510 Kea in Hawaii, which is operated by the University of Hawaii under Coopera-
511 tive Agreement no. NNX-08AE38A with the National Aeronautics and Space
512 Administration, Science Mission Directorate, Planetary Astronomy Program.
513 Support for this project was provided to N.M. by the Carnegie Institution of
514 Washington Department of Terrestrial Magnetism, the National Aeronautics
515 and Space Administration through the NASA Astrobiology Institute (NAI)
516 under Cooperative Agreement No. NNA04CC09A, and through the National
517 Science Foundation Astronomy and Astrophysics Postdoctoral Fellowship.

518 **References**

- 519 Abe, M. and 12 co-authors, 2006. Near-infrared spectral results of asteroid
520 Itokawa from the Hayabusa spacecraft. *Science* 312, 1334-1338.
- 521 Abe, S. and 16 co-authors, 2006. Mass and Local Topography Measurements
522 of Itokawa by Hayabusa. *Science* 312, 1344-1347.
- 523 Abe, M. and 24 co-authors, 2008. Ground-based observational campaign for
524 asteroid 162173 1999 JU3. *Lunar Planet. Sci.* 39. Abstract 1594.
- 525 Abell, P. A., Vilas, F., Jarvis, K. S., Gaffey, M. J., and Kelley, M. S., 2007.

Mineralogical composition of (25143) Itokawa 1998 SF36 from visible and near-infrared reflectance spectroscopy: Evidence for partial melting. *Met. Planet. Sci.* 42, 2165-2177.

Barucci, M. A. and 12 co-authors., 2012. Overview of Lutetia’s surface composition. *Planet. Space. Sci.* 66, 23-30.

Binzel, R. P., Harris, A. W., Bus, S. J., and Burbine, T. H., 2001a. Spectral Properties of Near-Earth Objects: Palomar and IRTF Results for 48 Objects Including Spacecraft Targets (9969) Braille and (10302) 1989 ML. *Icarus* 151, 139-149.

Binzel, R. P., Rivkin, A. S., Bus, S. J., Sunshine, J. M., and Burbine, T. H., 2001b. MUSES-C target asteroid (25143) 1998 SF36: A reddened ordinary chondrite. *Meteorit. Planet. Sci.* 36, 1167-1172.

Binzel, R. P., Morbidelli, A., Merouane, S., DeMeo, F. E., Birlan, M., Vernazza, P., Thomas, C. A., Rivkin, A. S., Bus, S. J., and Tokunaga, A. T. Earth encounters as the origin of fresh surfaces on near-Earth asteroids. *Nature* 463, 331-334.

Bobrovnikoff, N. T., 1929. The spectra of minor planets. *Lick Obs. Bull.* 14 (No. 407), 18-27.

Bus, S. J. and Binzel, R. P., 2002. Phase II of the Small Main-Belt Asteroid Spectroscopic Survey: A Feature-Based Taxonomy. *Icarus* 158, 146-177.

Campins, H., Emery, J. P., Kelley, M., Fernández, Y., Licandro, J., Delbó, M., Barucci, A., and Dotto, E., 2009. Spitzer observations of spacecraft target 162173 (1999 JU3). *A&A* 503, L17-L20.

Cloutis, E. A., Hiroi, T., Gaffey, M. J., Alexander, C. M. O’D., and Mann, P., 2011a. Spectral reflectance properties of carbonaceous chondrites: 1. CI chondrites. *Icarus* 212, 180-209.

Cloutis, E. A., Hudon, P., Hiroi, T., Gaffey, M. J., and Mann, P., 2011b. Spec-

553 tral reflectance properties of carbonaceous chondrites: 1. CM chondrites.
554 Icarus 216, 309-346.

555 Cushing, M. C., Vacca, W. D. and Rayner, J. T., 2004. Spextool: A Spec-
556 tral Extraction Package for SpeX, a 0.85.5 Micron Cross-Dispersed Spec-
557 trograph. PASP 116, 363-376.

558 de León, J., Mothé-Diniz, T., Licandro, J., Pinilla-Alonso, N., and Campins,
559 H., 2011. New observations of asteroid (175706) 1996 FG3, primary target
560 of the ESA Marco Polo-R mission. A&A 530, L12, 1-4.

561 DeMeo, F. E., Binzel, R. P., Slivan, S. M., and Bus, S. J., 2009. An extension
562 of the Bus asteroid taxonomy into the near-infrared. Icarus 202, 160-180.

563 Fujiwara, A. and 21 co-authors, 2006. The rubble-pile asteroid Itokawa as
564 observed by Hayabusa. Science 312, 1330-1334.

565 Gaffey, M. J., 1997. Surface lithologic heterogeneity of asteroid 4 Vesta. Icarus
566 127, 130-157.

567 Hasegawa, S. and 9 co-authors, 2008. Albedo, Size, and Surface Characteristics
568 of Hayabusa-2 Sample-Return Target 162173 1999 JU3 from AKARI and
569 Subaru Observations. Publ. Astron. Soc. Japan 60, S399-S405.

570 Hiroi, T., Zolensky, M. E., Pieters, C. M., and Lipschutz, M. E., 1996. Thermal
571 metamorphism of the C, G, B, and F asteroids seen from the 0.7 μ m, 3 μ m
572 and UV absorption strengths in comparison with carbonaceous chondrites.
573 Met. Planet. Sci. 31, 321-327.

574 Hiroi, T., Pieters, C. M., Zolensky, M. E., and Lipschutz, M. E., 1993. Evidence
575 of Thermal Metamorphism on the C, G, B, and F Asteroids. Science 261,
576 1016-1018.

577 Kawakami, K., Abe, M., Hasegawa, S., and Kasuga, T., 2010. Observation
578 of the post Hayabusa mission target asteroid (162173) 1999 JU3. Japanese
579 Society of Planetary Sciences 19, 4-11.

Kim, M.-J. and 9 co-authors, 2013. Optical observations of NEA 162173 (1999 JU3) during the 2011-2012 apparition. *A&A*, accepted for publication.

Landolt, A. U., 1992. UBVRI photometric standard stars in the magnitude range $11.5 < V < 16.0$ around the celestial equator. *AJ* 104, 340-371.

Lazzaro, D., Barucci, M. A., Perna, D., Jasmim, F. L., Yoshikawa, M., and Carvano, J. M. F., 2013. Rotational spectra of (162173) 1999 JU3, the target of the Hayabusa 2 mission. *A&A* 549, L2, 1-4.

Marchi, S., Delbó, M., Morbidelli, A., Paolicchi, P., and Lazzarin, M., 2009. Heating of near-Earth objects and meteoroids due to close approaches to the Sun. *Mon. Not. R. Astron. Soc.* 400, 147-153.

Michel, P. and Delbó, M., 2010. Orbital and thermal evolutions of four potential targets for a sample return space mission to a primitive near-Earth asteroid. *Icarus* 209, 520-534.

Morbidelli, A., Chambers, J., Lunine, J. I., Petit, J. M., Robert, F., Valsecchi, G. B., and Cyr, K. E., 2000. Source regions and timescales for the delivery of water to the Earth. *Met. Planet. Sci.* 35, 1309-1320.

Müller, T. G. and 17 co-authors, 2011. Thermo-physical properties of 162173 (1999 JU3), a potential flyby and rendezvous target for interplanetary missions. *A&A* 525, A145, 1-6.

Nakamura, T. and 21 co-authors, 2011. Itokawa Dust Particles: A Direct Link Between S-Type Asteroids and Ordinary Chondrites. *Science* 333, 1113-1116.

Pieters, C. M., 1983. Strength of Mineral Absorption Features in the Transmitted Component of Near-Infrared Reflected Light: First Results From RELAB. *J. Geophys. Res.* 88, 9534-9544.

Polishook, D. and 19 co-authors, 2012. Asteroid rotation periods from the Palomar Transient Factory survey. *Mon. Not. R. Astron. Soc.* 421, 2094-

2108.

Rayner, J., Toomey, D. W., Onaka, P. M., Denault, A. J., Stahlberger, W. E.,
 Vacca, W. D., and Cushing, M. C., 2003. SpeX: A Medium-Resolution 0.85.5
 Micron Spectrograph and Imager for the NASA Infrared Telescope Facility.
 PASP 115, 362-382.

Reddy, V. and 24 co-authors, 2012a. Color and albedo heterogeneity of Vesta
 from Dawn. *Science* 336, 700-704.

Reddy, V., Gaffey, M. J., Abell, P. A., and Hardersen, P. S., 2012b. Constraining
 albedo, diameter and composition of near-Earth asteroids via near-IR
 spectroscopy. *Icarus* 219, 382-392.

Reddy, V., Le Corre, L., Hicks, M., Lawrence, K., Buratti, B., Abell, P., Gaffey,
 M. J., and Hardersen, P. S., 2012c. Composition of near-Earth asteroid 2008
 EV5: Potential target for robotic and human exploration. *Icarus* 221, 678-
 681.

Reddy, V. and 11 co-authors, 2012d. Photometric, spectral phase and temperature
 effects on Vesta and HED meteorites: Implications for Dawn mission.
Icarus 217, 153-168.

Richardson, J. E., Melosh, H. J. and Greenberg, R., 2004. Impact-Induced
 Seismic Activity on Asteroid 433 Eros: A Surface Modification Process.
Science 306, 1526-1529.

Rivkin, A. S., Howell, E. S., Vilas, F., and Lebofsky, L. A., 2002. Hydrated
 minerals on asteroids: The astronomical record. In: Bottke, W. F., Cellino,
 A., Paollicchi, P., Binzel, R. P. (Eds.), *Asteroids III*. Univ. Arizona Press,
 Tucson, pp. 235-253.

Saito, J. and 33 co-authors, 2006. Detailed images of asteroid 25143 Itokawa
 from Hayabusa. *Science* 312, 1341-1344.

Sanchez, J. A., Reddy, V., Nathues, A., Cloutis, E. A., Mann, P., and

634 Hiesinger, H., 2012. Phase reddening on near-Earth asteroids: Implications
 635 for mineralogical analysis, space weathering and taxonomic classification.
 636 *Icarus* 220, 36-50.

637 Sugita, S., Kuroda, D., Kameda, S., Hasegawa, S., Kamata, S., Abe, M., Ishig-
 638 uro, M., Takato, N., and Yoshikawa, M., 2012. Visible spectroscopic observa-
 639 tion of asteroid 162173 (1999 JU3) with the Gemini-S telescope. American
 640 Astronomical Society, 44th DPS meeting, Abstract 102.02.

641 Sunshine, J. M., Bus, S. J., McCoy, T. J., Burbine, T. H., Corrigan, C. M.,
 642 and Binzel, R. P., 2004. High-calcium pyroxene as an indicator of igneous
 643 differentiation in asteroids and meteorites. *Meteorit. Planet. Sci.* 39, 1343-
 644 1357.

645 Tonui, E. K., Zolensky, M. E., Lipschutz, M. E., Wang, M.-S., and Nakamura,
 646 T., 2003. Yamato 86029: Aqueously altered and thermally metamorphosed
 647 CI-like chondrite with unusual textures. *Met. Planet. Sci.* 38, 269-292.

648 Vernazza, P., Brunetto, R., Binzel, R. P., Perron, C., Fulvio, D., Strazzulla, G.,
 649 and Fulchignoni, M., 2009. Plausible parent bodies for enstatite chondrites
 650 and mesosiderites: Implications for Lutetias fly-by. *Icarus* 202, 477-486.

651 Vilas, F. and Sykes, M., 1996. Are low-albedo asteroids thermally metamor-
 652 phosed?. *Icarus* 124, 483-489.

653 Vilas, F., 2008. Spectral characteristics of Hayabusa 2 near-Earth asteroid
 654 targets 162173 1999 JU3 and 2001 QC34. *AJ* 135, 1101-1105.

655 Vilas, F., 2012. New spectral reflectance observations of Hayabusa 2 near-
 656 Earth asteroid target 162173 1999 JU3. American Astronomical Society,
 657 44th DPS meeting, Abstract 102.03.

UT Date	Instrument and Facility	V	Δ (AU)	R (AU)	α ($^\circ$)	ϱ	T-O-M ($^\circ$)	Solar Analogs
1999-05-17 [†]	DSPEC Palomar 200''	17.7	0.305	1.314	6.1	5%	149	SA102-1081, 16 Cyg B
2007-07-11 [‡]	RCHAN MMT 6.5m	20.3	0.569	1.381	40.3	12%	78	SA114-654
2007-09-10 [‡]	RCHAN MMT 6.5m	17.9	0.273	1.254	22.5	2%	150	SA114-654
2007-09-11 [‡]	RCHAN MMT 6.5m	17.9	0.271	1.251	22.8	0%	152	SA113-276, SA114-654
2007-09-18	SpeX IRTF	17.9	0.260	1.231	26.5	37%	90	SA112-1333, SA115-271, SA93-101, Hya64
2007-09-20	SpeX IRTF	17.9	0.258	1.226	27.9	56%	68	SA110-361, SA112-1333, SA115-271, SA93-101
2012-06-01	LDSS3 Magellan 6.5m	17.7	0.353	1.367	0.2	85%	45	SA110-361, HD149182
2012-06-02	LDSS3 Magellan 6.5m	17.8	0.354	1.368	1.0	92%	31	HD149182
2012-06-03	LDSS3 Magellan 6.5m	17.9	0.356	1.370	2.0	98%	15	SA107-998
2012-06-05	FIRE Magellan 6.5m	18.1	0.360	1.373	4.4	99%	15	SA107-998
2012-07-10	FIRE Magellan 6.5m	19.9	0.518	1.410	33.1	60%	127	SA113-276

Table 1: Chronological summary of spectroscopic observations of 1999 JU3.

The columns in this table are the UT date of observation, the instrument and facility that were used, the apparent V-band magnitude (from the Minor Planet Center), geocentric distance (Δ), heliocentric distance (R), the solar phase angle (α), the phase of the moon (\mathcal{C}), the target-observer-Moon angle (T-O-M), and the solar analog stars used for calibration. The first four entries are from [†]Binzel et al. (2001a) or [‡]Vilas (2008).

UT Date	Instrument and Facility	V	Δ (AU)	R (AU)	α ($^\circ$)
2011-10-30	EEV 1k CCD Lulin 1m	20.1	0.438	1.002	76.1
2012-04-05	IMACS Magellan 6.5m	19.8	0.461	1.237	49.4
2012-04-06	IMACS Magellan 6.5m	19.8	0.457	1.240	48.9
2012-04-07	IMACS Magellan 6.5m	19.8	0.454	1.243	48.5
2012-05-31	SITe1k Tenagra 0.8m	17.7	0.352	1.366	0.7
2012-06-07	SITe1k Tenagra 0.8m	18.2	0.366	1.377	7.1
2012-06-08	SITe1k Tenagra 0.8m	18.3	0.368	1.378	8.2
2012-06-09	SITe1k Tenagra 0.8m	18.4	0.371	1.380	9.2
2012-06-20	Tek1k Bosque Alegre 1.5m	19.0	0.409	1.393	19.4
2012-06-21	Tek1k Bosque Alegre 1.5m	19.0	0.413	1.394	20.3

Table 2: Summary of 1999 JU3 photometric observations.
The columns in this table are the same as in Table 2.

UT Midpoint	Reference	V	Δ (AU)	R (AU)	α ($^\circ$)	Sub-Observer Long. and Lat.
Müller et al. (2011) Shape Model						
1999-05-17 07:49	B01	17.7	0.305	1.314	6.1	$-169^\circ, 19^\circ$
2007-07-11 10:05	V08	20.3	0.569	1.381	40.3	$-40^\circ, 8^\circ$
2007-09-10 07:00	V08	17.9	0.273	1.254	22.5	$169^\circ, 25^\circ$
2007-09-11 05:50	V08	17.9	0.271	1.251	22.8	$172^\circ, 25^\circ$
2012-06-01 07:07	A	17.7	0.353	1.367	0.2	$158^\circ, 27^\circ$
2012-06-01 08:09	B	17.7	0.353	1.367	0.2	$109^\circ, 28^\circ$
2012-06-02 03:54	C	17.8	0.354	1.368	1.0	$-102^\circ, 28^\circ$
2012-06-03 01:54	D	17.9	0.356	1.370	2.0	$-59^\circ, 28^\circ$
2012-06-03 03:34	E	17.9	0.356	1.370	2.1	$-137^\circ, 28^\circ$
2012-06-03 04:54	F	17.9	0.356	1.370	2.2	$159^\circ, 28^\circ$
Kawakami et al. (2010) Shape Model						
1999-05-17 07:49	B01	17.7	0.305	1.314	6.1	$-19^\circ, 10^\circ$
2007-07-11 10:05	V08	20.3	0.569	1.381	40.3	$25^\circ, -71^\circ$
2007-09-10 07:00	V08	17.9	0.273	1.254	22.5	$-61^\circ, -77^\circ$
2007-09-11 05:50	V08	17.9	0.271	1.251	22.8	$-57^\circ, -78^\circ$
2012-06-01 07:07	A	17.7	0.353	1.367	0.2	$-34^\circ, -9^\circ$
2012-06-01 08:09	B	17.7	0.353	1.367	0.2	$-83^\circ, -9^\circ$
2012-06-02 03:54	C	17.8	0.354	1.368	1.0	$65^\circ, -9^\circ$
2012-06-03 01:54	D	17.9	0.356	1.370	2.0	$107^\circ, -8^\circ$
2012-06-03 03:34	E	17.9	0.356	1.370	2.1	$29^\circ, -8^\circ$
2012-06-03 04:54	F	17.9	0.356	1.370	2.2	$-35^\circ, -8^\circ$

Table 3: Sub-observer points for all published visible-wavelength spectra of 1999 JU3.

Columns in this table are the UT midpoint of observation, reference [B01 = Binzel et al. (2001a); V08 = Vilas (2008); letters A-F indicate the corresponding spectra in Figure 1], solar phase angle (α), and the sub-observer longitude and latitude. These data are presented for both shape models of 1999 JU3.

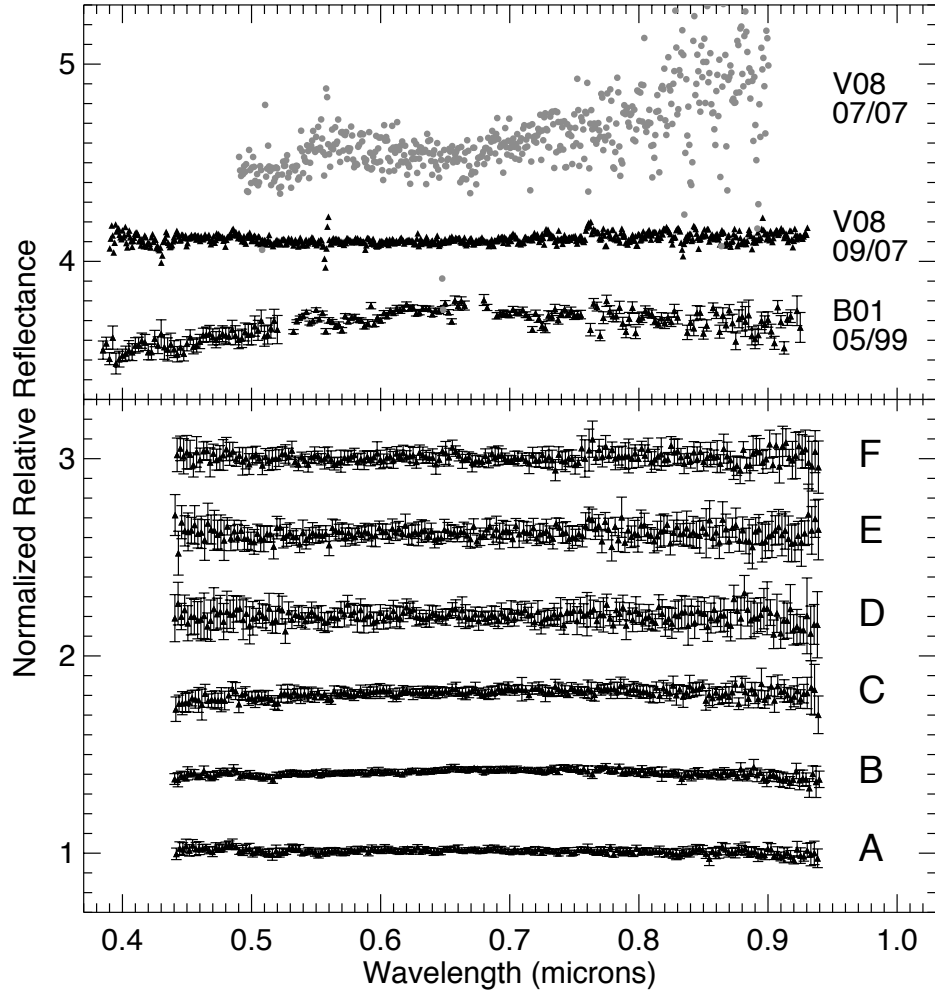


Fig. 1. Normalized visible-wavelength reflectance spectra of 1999 JU3. The data are vertically offset for clarity. The top panel shows the three previous visible spectra with the month/year of observation and respective references B01 = Binzel et al. (2001a) and V08 = Vilas (2008). The July 2007 data is shown in grey to distinguish it from the adjacent spectrum. Our spectra are in the bottom panel and are chronologically ordered from bottom to top with spectra A and B taken on June 1, C on June 2, and D-F taken on June 3. The midpoint times for each of these observations are given in Table 3. The progressive decrease in signal-to-noise in spectra A-F is due to the opposition effect, increasing geocentric and heliocentric distances, and increasing background from a waxing moon.

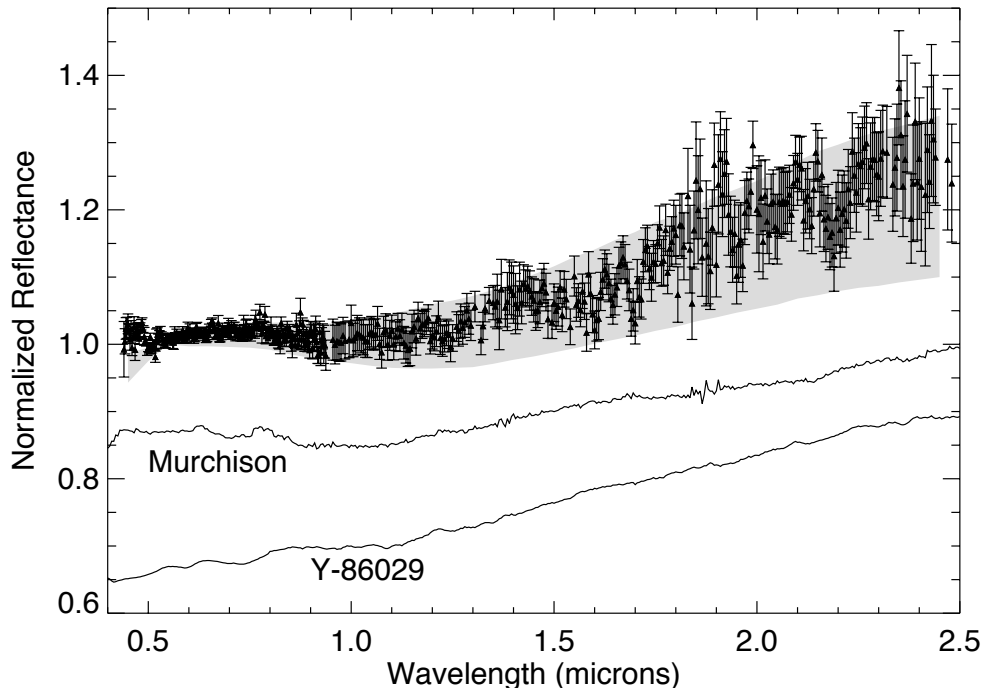


Fig. 2. Composite visible (LDSS3) and near-infrared (SpeX and FIRE) spectrum of 1999 JU3. The grey region in the background represents the envelope for C-type spectra in the DeMeo et al. (2009) taxonomic system. In spite of the low signal-to-noise in the near-infrared and the presence of residual telluric features around 1.4 and 1.9 μm , this spectrum shows no evidence for prominent absorption bands, though subtle features may be present around 0.9 μm and short-ward of 0.7 μm . The two best spectral matches from our χ^2 search through RELAB are a thermally altered sample of Murchison and the unusual CI chondrite Yamato 86029. These meteorite spectra have been normalized at 1 μm and then offset by -0.15 and -0.3 units respectively.

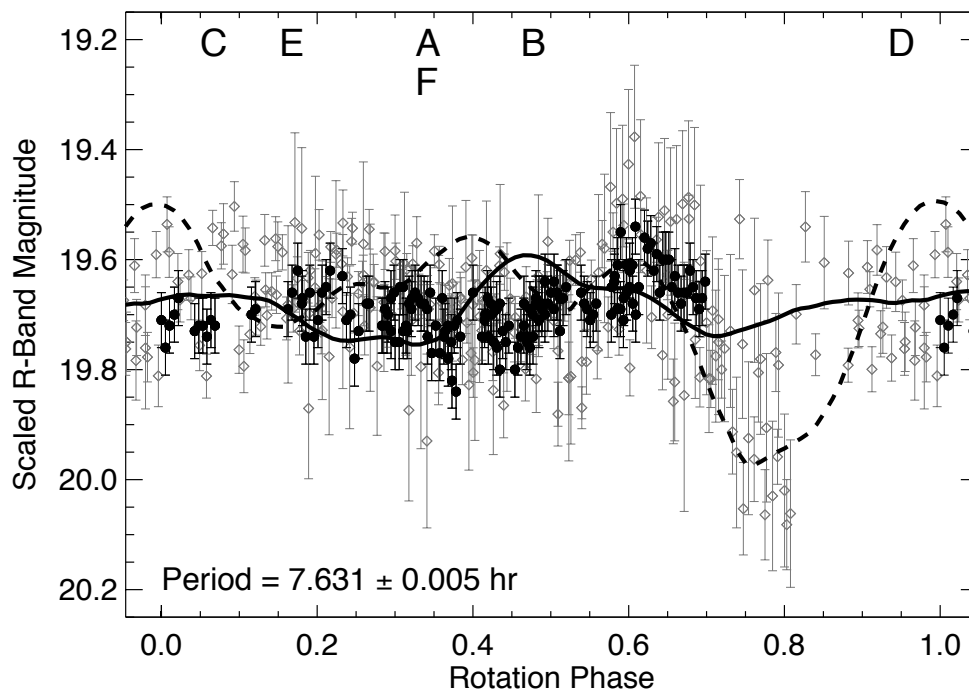


Fig. 3. Rotational light curve of 1999 JU3. Filled circles represent the IMACS Magellan data. Open diamonds represent our additional observations (Table 2) with magnitudes scaled to the IMACS data. The solid line represents the predicted light curve from the Müller et al. (2011) model, the dashed is the model prediction from Kawakami et al. (2010). The data have been phase folded to a synodic period of 7.631 hours. A rotation phase of zero corresponds to the start of IMACS observations on UT 2012-04-05 at 06:40 (JD 2456022.778). The phases accessed by the visible-wavelength spectroscopic observations are indicated by the letters A-F. The total time for each spectrum (4 x 180 seconds plus readout and telescope offsets) is comparable to the width of the letters. Spectroscopic coverage was obtained over approximately 60% of rotation phases at a longitudinal resolution of $\sim 45^\circ$.

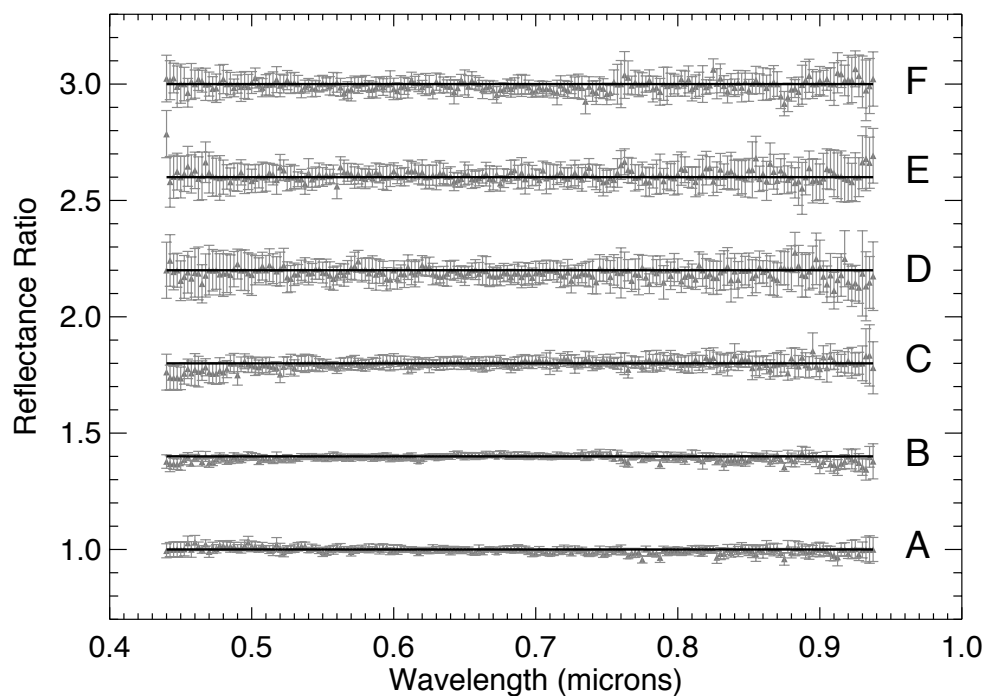


Fig. 4. Visible-wavelength reflectance ratios of 1993 JU3 relative to a median combination of all spectra. These reflectance ratios have been offset by multiples of 0.4 units. Deviations from a slope-zero line (black curves) would indicate spectroscopic heterogeneity. No variability is detected within the S/N of the data, though slight ($< 4\%$) deviations from a flat line are seen at the shortest wavelengths in spectra B and C.

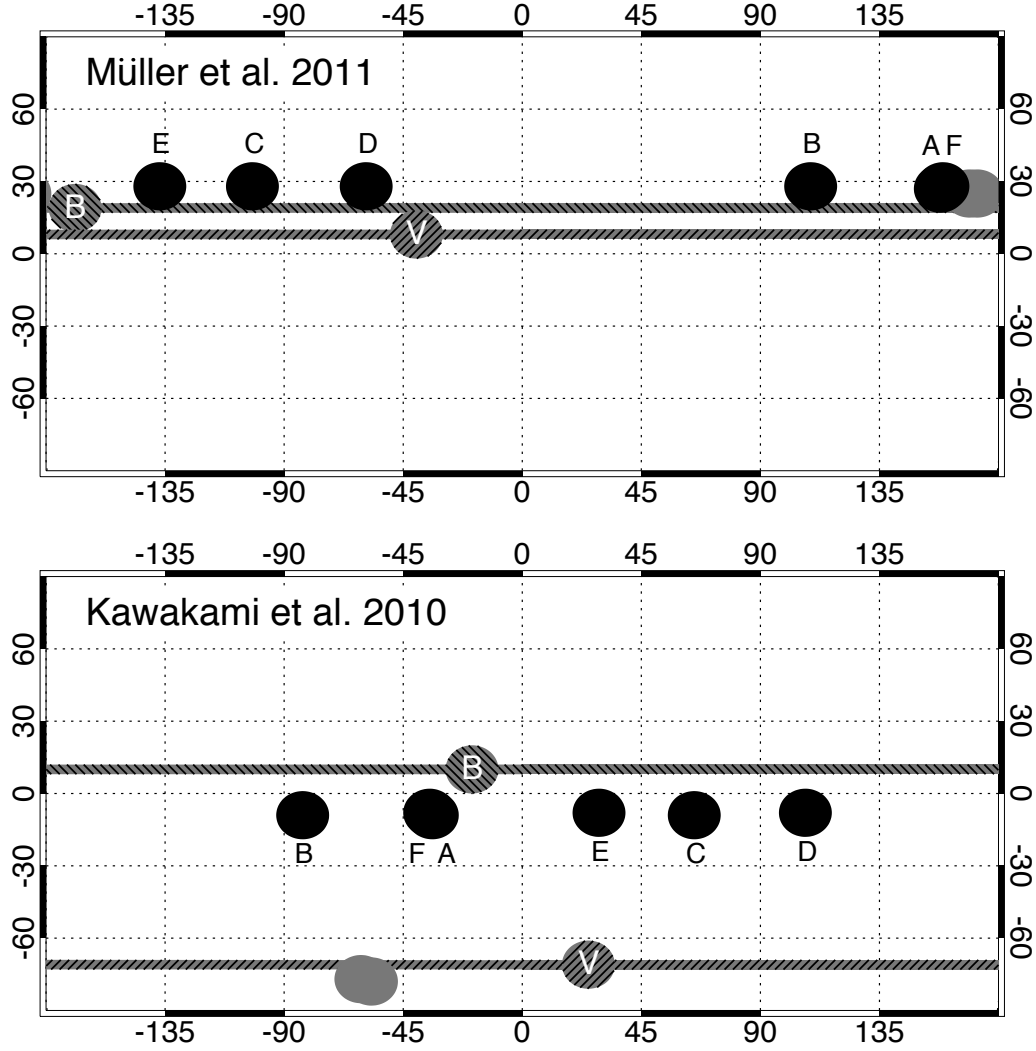


Fig. 5. Cylindrical projections of 1999 JU3's surface with circles indicating the sub-observer latitudes and longitudes from the two available shape models (Kawakami et al., 2010; Müller et al., 2011). The circles are not meant to indicate the physical extent of the surface accessed by the observations. Black circles represent sub-observer points from our new 2012 observations and are labeled A-F. Grey circles represent sub-observer points for the observations from 1999 and 2007. The two spectra that display absorption features are indicated with hatched regions and labeled B (Binzel et al., 2001a) and V (Vilas, 2008). Surface regions that produce absorption features must be limited in extent to avoid overlapping those corresponding to featureless spectra. The loss of rotational information across epochs (see text) suggests that the locations of these regions relative to the 2012 points could lie anywhere along the horizontal bands. This demands that any heterogeneity on the surface be confined to regions no more than a few hundred meters in extent.

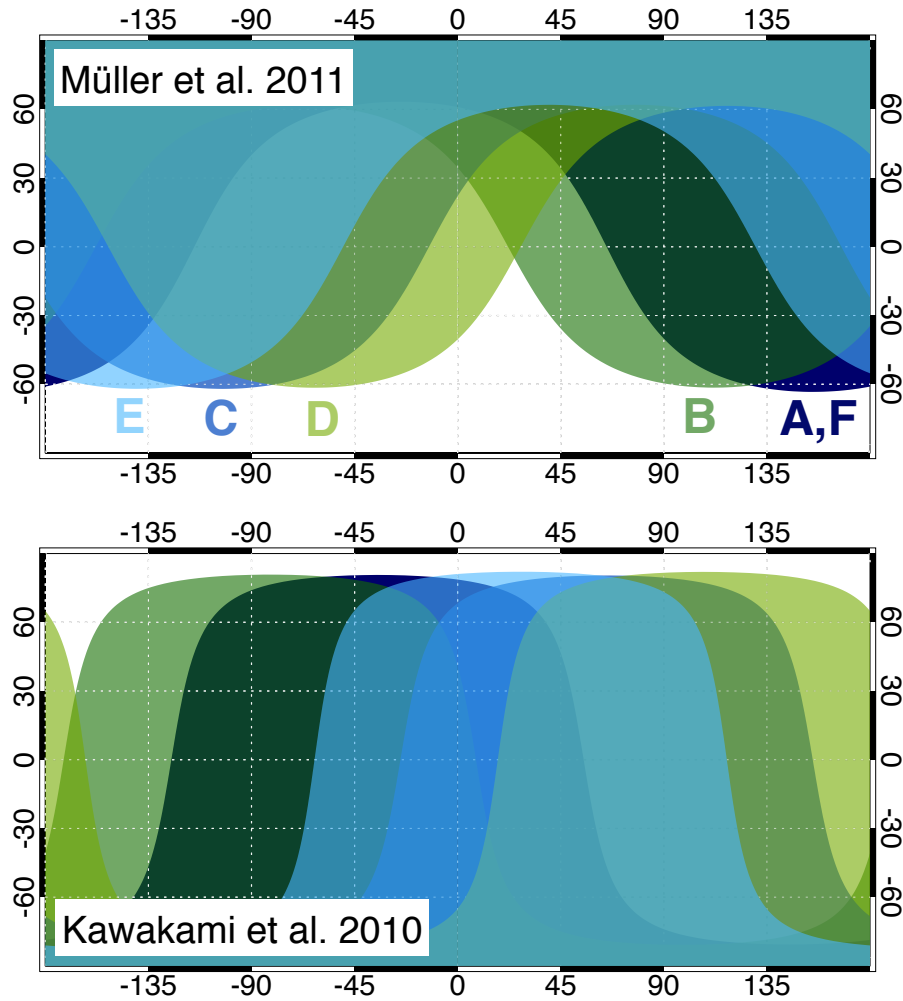


Fig. 6. SUPPLEMENTARY ONLINE FIGURE: Cylindrical projection of 1999 JU3's surface with sub-observer hemispherical footprints indicating the regions accessed by our spectra A-F. Projections are shown for both the Müller et al. (2011) and Kawakami et al. (2010) shape models. The hemispherical regions are color coded for each spectrum as indicated by the letters in the top panel. The sub-observer hemispheres for spectra A and F are so similar that they have been combined into a single dark blue region. The sub-observer points in Figure 5 would lie at the center of their respective regions. The Vilas (2008) and Binzel et al. (2001a) hemispheres are not plotted, but it is clear that they would almost entirely overlap with the regions here. Our spectra obtained hemispherical averages over a majority of the asteroid's surface, independent of which shape model is assumed, thus leaving little room for heterogenous regions that could produce prominent spectral absorption bands.